ELSEVIER

Journal of Quantitative Spectroscopy & Radiative Transfer 92 (2005) 9–30

Journal of Quantitative Spectroscopy & Radiative Transfer

www.elsevier.com/locate/jqsrt

Control volume finite element method for radiation

M. Ben Salah[a,*], F. Askri[a], D. Rousse[b], S. Ben Nasrallah[a]

[a]*Laboratoire d'Etudes des Systèmes Thermiques et Energétiques, Ecole Nationale d'Ingénieurs de Monastir, Avenue Ibn EI Jazzar, 5019 Monastir, 5000, Tunisia*

[b]*Département de génie mécanique, Université Laval, Cité Universitaire, Qué., Canada G1K 7P4*

Received 17 October 2003; accepted 16 July 2004

Abstract

In this paper a new methodology is presented by the authors for the numerical treatment of radiative heat transfer in emitting, absorbing and scattering media. This methodology is based on the utilisation of Control Volume Finite Element Method (CVFEM) and the use, for the first time, of matrix formulation of the discretized Radiative Transfer Equation (RTE). The advantages of the proposed methodology is to avoid problems that confronted when previous techniques are used to predict radiative heat transfer, essentially, in complex geometries and when there is scattering and/or non-black boundaries surfaces. Besides, the new formulation of the discretized RTE presented in this paper makes it possible to solve the algebraic system by direct or iterative numerical methods. The theoretical background of CVFEM and matrix formulation is presented in the text. The proposed technique is applied to different test problems, and the results compared favourably against other published works. Moreover this paper discusses in detail the effects of some radiative parameters, such as optical thickness and walls emissivities on the spatial evolution of the radiant heat flux. The numerical simulation of radiative heat transfer for different cases using the algorithm proposed in this work has shown that the developed computer procedure needs an accurate CPU time and is exempt of any numerical oscillations.

Keywords: ETR; CVFEM; Matrix resolution; Radiative heat transfer

*Corresponding author. Tel.: 216-73-500-244; fax: 216-73-500-514.
E-mail address: mohieddine2002@yahoo.com (M.B. Salah).

0022-4073/$ - see front matter © 2004 Elsevier Ltd. All rights reserved.
doi:10.1016/j.jqsrt.2004.07.008

1. Introduction

Radiative heat transfer coupled with conduction, convection and fluid dynamics appears in many engineering high-temperature systems, such as furnaces, boilers, combustion chamber, heat exchangers and nuclear reactors. Efficient design of these systems requires a simultaneous solution of the fluid dynamics, heat and mass transfer and essentially the radiative heat process. This means that numerical procedures are necessary to solve the Radiative Transfer Equation (RTE) and should: (i) permit compatibility with available methods that used for the fluid dynamics and convection–conduction heat transfer; (ii) allow geometrical flexibility; and (iii) require an accurate computational time and storage capacity.

Several methods have been developed for solving the RTE. But, the majority of these methods appear to have little in common with methods of computational fluid dynamics (CFD). For example, Zone Method [1,2] and Monte Carlo Method [3–5] have long been accepted as the most accurate methods for the calculation of radiative heat transfer. However, it is now well established that both these methods have been proved difficult to incorporate in other discrete numerical methods of CFD and that they require a large amount of computational time and storage capacity. The Discrete Transfer Method [6] offers several interesting features as it incorporates key ideas of the Zonal, Monte Carlo and Flux Method. In a paper by Meng et al. [7], the authors successfully implemented the Discrete Transfer Method on an unstructured mesh, but confirmed the conclusion reported by Carvalho et al. [8], the method does not yet provide high accuracy for scattering media and it also foreign to CFD analysis. The Discrete Ordinates Method [9,10] applies spatial discretization exactly as in CFD, but the quadrature integration over direction has no fluid flow or convective transfer counterpart. The Finite Volume Method (FVM) [11], and recently the Control Volume Finite Element Method (CVFEM) [12] allow radiation to be treated in a way that is familiar to a CFD specialist. In fact, these methods share the same philosophy and computational grid as the fluid dynamics and convection–conduction heat transfer approach. However, when there is scattering and/or non-black boundaries surfaces, the source term of the discretized radiative transfer equation obtained by FVM and CVFEM, is not temperature dependent only, but also it depends on radiation intensity. Consequently, for these two methods, an iterative techniques (Three Diagonal Matrix Algorithm (TDMA) [13], marching process [14–17]) in which source term is computed using the latest available values of intensities, was necessary to solve the algebraic system. This dependence of the source term on solution provoked, in some cases, oscillations and/or divergence in iterative process. Besides, the computer procedure requires a long CPU time.

So the aim objective of this paper is to use the CVFEM approach to discretize the RTE and to propose a new formulation that makes it possible to use direct methods (Gauss Method, matrix inversion) or iterative methods (Jaccobi Method, Gauss Seidel Method, Conjugate Gradient Methods) for numerical resolution of discretized RTE.

A computer procedure is developed and tested for different radiation problems, and the results present a good agreement with other available works. The method accounts for absorption, emission and scattering and proves to be very accurate and of good flexibility. Furthermore, this approach permits compatibility with other numerical method used for CFD problems.

2. Basic equations

The RTE in an absorbing, emitting and scattering grey medium can be written as

$$\vec{\nabla}\cdot(I(s,\vec{\Omega})\cdot\vec{\Omega}) = -(k_a+k_d)I(s,\vec{\Omega}) + k_a I_b(s) + \frac{k_d}{4\pi}\int_{\Omega'=4\pi} I(s,\vec{\Omega}')\Phi(\vec{\Omega}'\to\vec{\Omega})\,d\Omega', \quad (1)$$

where $I(s,\vec{\Omega})$ is the radiative intensity, which is a function of position s and direction $\vec{\Omega}$; k_a and k_d are absorption and scattering coefficients, respectively; $I_b(s)$ is the blackbody radiative intensity at the temperature of the medium; and $\Phi(\vec{\Omega}'\to\vec{\Omega})$ is the scattering phase function from the incoming $\vec{\Omega}'$ direction to the outgoing direction $\vec{\Omega}$. The term on the left-hand side represents the gradient of the intensity in the direction $\vec{\Omega}$. The three terms on the right-hand side represent the changes in intensity due to absorption and out-scattering, emission, and in-scattering, respectively.

The radiative boundary condition for Eq. (1), when the wall bounding the physical domain is assumed grey and emits and reflects diffusely, can be expressed as

$$I_w(\vec{\Omega}) = \frac{\varepsilon_w\sigma T_w^4}{\pi} + \frac{1-\varepsilon_w}{\pi}\int_{\vec{\Omega}'\cdot\vec{n}_w<0} I_w(\vec{\Omega}')\left|\vec{\Omega}'\cdot\vec{n}_w\right| d\Omega' \quad \text{if } \vec{\Omega}\cdot\vec{n}_w>0, \quad (2)$$

where ε_w is the wall emissivity and $\vec{n}_w$ represents the unit normal vector on the wall (Fig. 1).

3. Numerical procedure

3.1. Discretization

The CVFEM is used to discretize the RTE. In the CVFEM, the spatial and angular domains are divided into a finite number of control volumes and control solid angles, respectively.

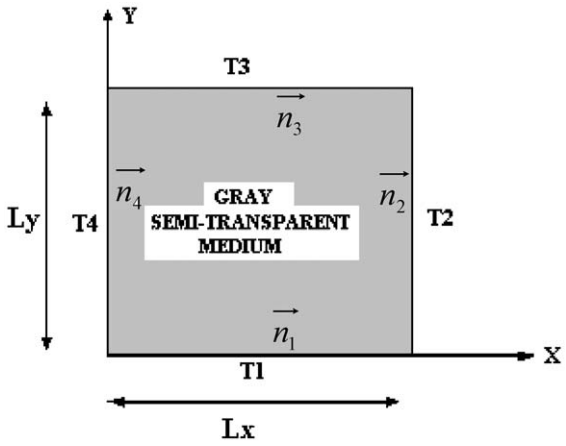

Fig. 1. Physical domain (rectangular cavity filled with grey semi-transparent medium).

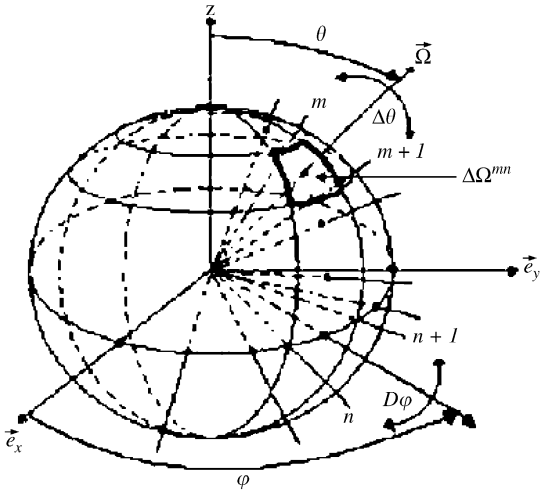

Fig. 2. Angular discretization (control solid angle $\Delta\Omega^{mn}$).

The total solid angle is subdivided into $N_\theta N_\varphi$ control solid angles as depicted in Fig. 2, where $\Delta\theta = \pi/N_\theta$ and $\Delta\varphi = 2\pi/N_\varphi$. The N_θ and N_φ represent numbers of control angle in the polar angle θ and azimuthal angle φ directions, respectively. These $N_\theta N_\varphi$ control solid angles are non-overlapping, and their sum is 4π.

The control solid angle $\Delta\Omega^{mn}$ is defined (Fig. 2) by the angular ranges $\lfloor m\Delta\theta, (m+1)\Delta\theta\rfloor$ and $\lfloor n\Delta\varphi, (n+1)\Delta\varphi\rfloor$, and is expressed by

$$\Delta\Omega^{mn} = \int_{m\Delta\theta}^{(m+1)\Delta\theta} \int_{n\Delta\varphi}^{(n+1)\Delta\varphi} \sin\,\theta\,\mathrm{d}\theta\,\mathrm{d}\varphi. \tag{3}$$

The spatial domain is subdivided into three-node triangular elements. As shown in Fig. 3a, a control volume ΔV_{ij} is created around each node N by enjoining the controids G_l of the elements to midpoints M_l and M_{l+1} of the corresponding sides. Each element has two faces, M_lG_l and G_lM_{l+1}, bounding the subcontrol volume around N, and each control volume is constructed by adding all subvolumes $NM_lG_lM_{l+1}N$.

In order to avoid the problem of sudden change of temperature between the boundaries and the medium and to use the minimum of calculation nodes, a specific function f, is used to obtain a non uniform mesh in which a very fine grid in the vicinity of the surfaces is released (Fig. 3a). The obtained mesh is composed of N_xN_y non equal control volumes ΔV_{ij}. The N_x and N_y represent numbers of nodes in x and y direction, respectively. And

$$\Delta x_i = \Delta x f(N_x, i), \quad \Delta y_j = \Delta y f(N_y, j), \tag{4}$$

where Δx and Δy represent the regular steps in x and y direction, respectively, and they are given by: $\Delta x = L_x/(N_x - 1), \Delta y = L_y/(N_y - 1)$ with L_x and L_y are, respectively, the x and y dimensions of the calculation domain (Fig. 1).

Integrating Eq. (1) over the control volume ΔV_{ij} (Fig. 3a) and the control solid angle $\Delta\Omega^{mn}$ (Fig. 2), and transforming the volume integral of gradient intensity term to a surface integral by

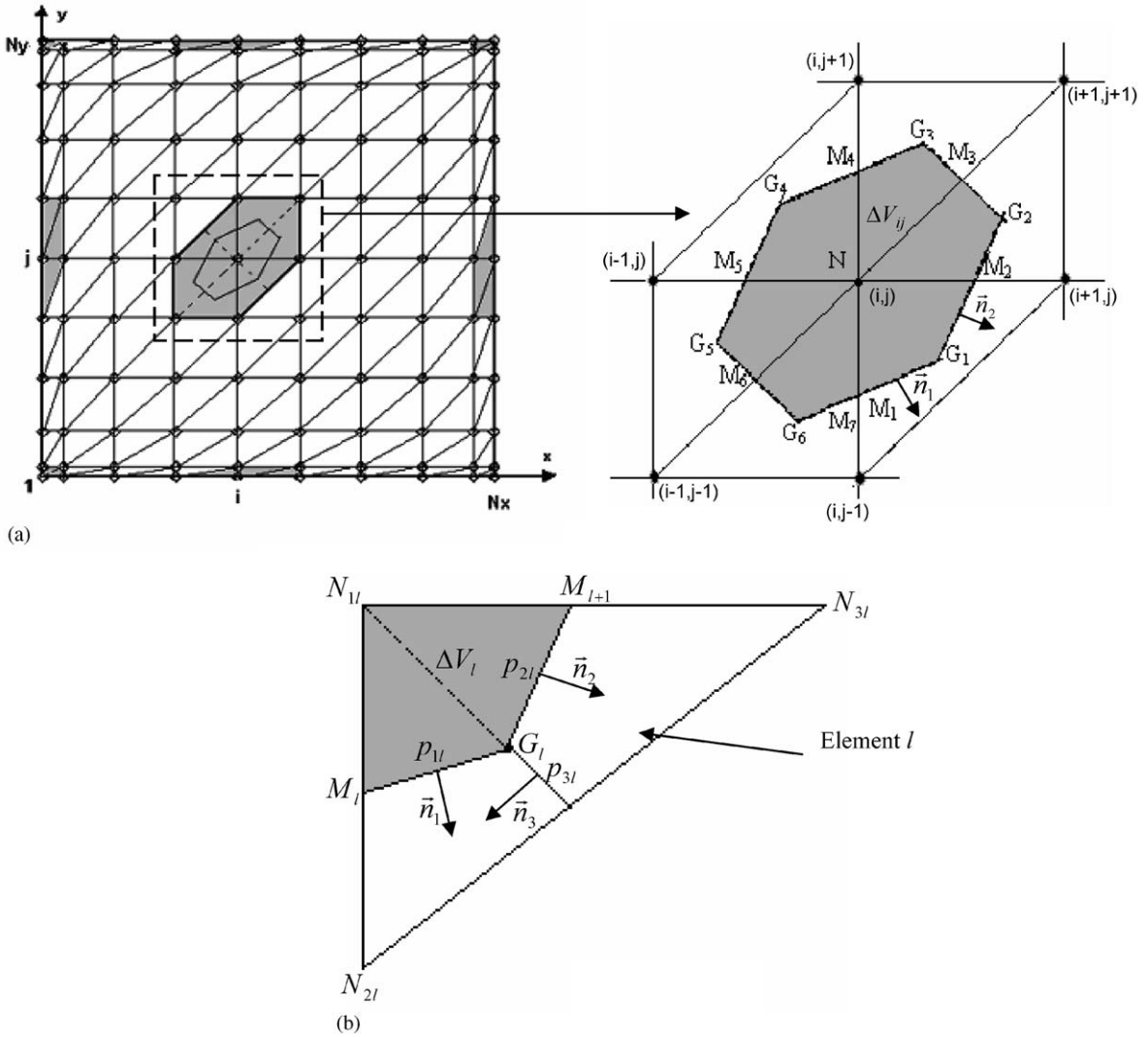

Fig. 3. Spatial-discretization (control volume ΔV_{ij}).

the divergence theorem, Eq. (1) then becomes:

$$\sum_{l=1}^{6}\left[\int_{\Delta\Omega^{mn}}\int_{M_l}^{G_l}\boldsymbol{J}\cdot\boldsymbol{n}\,\mathrm{d}s\,\mathrm{d}\Omega+\int_{\Delta\Omega^{mn}}\int_{G_l}^{M_{l+1}}\boldsymbol{J}\cdot\boldsymbol{n}\,\mathrm{d}s\,\mathrm{d}\Omega\right]_N$$
$$=-\int_{\Delta V_{ij}}\int_{\Delta\Omega^{mn}}(k_\mathrm{a}+k_\mathrm{d})I(s,\vec{\Omega})\,\mathrm{d}\Omega\,\mathrm{d}v$$
$$+\int_{\Delta V_{ij}}\int_{\Delta\Omega^{mn}}k_\mathrm{a}I_\mathrm{b}(s)\,\mathrm{d}\Omega\,\mathrm{d}v+\frac{k_\mathrm{d}}{4\pi}\int_{\Delta V_{ij}}\int_{\Delta\Omega^{mn}}\left(\int_{\Omega'=4\pi}I(s,\vec{\Omega}')\Phi(\vec{\Omega}'\to\vec{\Omega})\,\mathrm{d}\Omega'\right)\mathrm{d}\Omega\,\mathrm{d}v,\quad(5)$$

where $\boldsymbol{J} = I\vec{\Omega}$, l is the number of each element, and $\boldsymbol{n}$ is a unit outward vector normal to the differential length element ds.

The radiation intensity I is assumed to be constant over an entire solid angle $\Delta\Omega^{mn}$ and it is represented by I^{mn}. Thus, the surfaces and angular integrals of the intensity in the integral conservation equation (Eq. (5)) is approximated by

$$\sum_{l=1}^{6}\left[\int_{\Delta\Omega^{mn}}\int_{M_l}^{G_l}\boldsymbol{J}\cdot\boldsymbol{n}\,\mathrm{d}s\,\mathrm{d}\Omega+\int_{\Delta\Omega^{mn}}\int_{G_l}^{M_{l+1}}\boldsymbol{J}\cdot\boldsymbol{n}\,\mathrm{d}s\,\mathrm{d}\Omega\right]_N = \sum_{l=1}^{6}\left[G_{1lN}^{mn}\left[\int_{M_l}^{G_l}I^{mn}\,\mathrm{d}s\right]_N+G_{2lN}^{mn}\left[\int_{G_l}^{M_{l+1}}I^{mn}\,\mathrm{d}s\right]_N\right], \tag{6}$$

where

$$G_{klN}^{mn}=\int_{\Delta\Omega^{mn}}\vec{\Omega}\cdot\vec{n}_{klN}\,\mathrm{d}\Omega,\quad k=1,2,3.$$

The subscript N represents the central node of the control volume.

To approximate the integral of the intensity I^{mn} over each of the control volume surfaces (panels) within an element (Fig. 3b), the intensity is evaluated at the centroid of the panel and it is assumed to prevail over it. Then Eq. (6) becomes:

$$\sum_{l=1}^{6}\left[G_{1lN}^{mn}\left[\int_{M_l}^{G_l}I^{mn}\,\mathrm{d}s\right]_N+G_{2lN}^{mn}\left[\int_{G_l}^{M_{l+1}}I^{mn}\,\mathrm{d}s\right]_N\right]=\sum_{l=1}^{6}[G_{1lN}^{mn}A_{1l}^{N}I_{p1l}^{mn}+G_{2lN}^{mn}A_{2l}^{N}I_{p2l}^{mn}], \tag{7}$$

where $A_{1l}^{N}=M_lG_l$ and $A_{2l}^{N}=G_lM_{l+1}$.

To approximate the integrals that represent the extinction, in-scattering and emission contributions over the control volume ΔV_{ij} and the control solid angle $\Delta\Omega^{mn}$, the radiation intensity is evaluated at the centroid of the control volume and at the centre direction of the control solid angle and it is assumed to prevail over its. Then, extinction, in-scattering and emission terms in Eq. (5) are, respectively, expressed by the following expressions:

$$\int_{\Delta V_{ij}}\int_{\Delta\Omega^{mn}}(k_\mathrm{a}+k_\mathrm{d})I(s,\vec{\Omega})\,\mathrm{d}\Omega\,\mathrm{d}v=(C_{\mathrm{ex}}^{mn})_{ij}I_{ij}^{mn}, \tag{8}$$

$$-\frac{k_\mathrm{d}}{4\pi}\int_{\Delta V_{ij}}\int_{\Delta\Omega^{mn}}\left(\int_{\Omega'=4\pi}I(s,\vec{\Omega}')\Phi(\vec{\Omega}'\to\vec{\Omega})\,\mathrm{d}\Omega'\right)\mathrm{d}\Omega\,\mathrm{d}v=\sum_{m',n'}^{N_\theta\times N_\varphi}[(C_{\mathrm{diff}}^{mnm'n'})_{ij}I_{ij}^{m'n'}], \tag{9}$$

$$\int_{\Delta V_{ij}}\int_{\Delta\Omega^{mn}}K_\mathrm{a}I_\mathrm{b}(s)\,\mathrm{d}\Omega\,\mathrm{d}v=(C_{\mathrm{em}}^{mn})_{ij}I_{bij}^{mn}, \tag{10}$$

where

$$I_{bij}^{mn} = \frac{\sigma T_{ij}^4}{\pi}, \tag{11}$$

$$(C_{\text{ex}}^{mn})_{ij} = (k_{\text{a}} + k_{\text{d}})\Delta\Omega^{mn}\Delta V_{ij}, \tag{12}$$

$$(C_{\text{diff}}^{mnm'n'})_{ij} = -\frac{k_{\text{d}}}{4\pi}\Delta\Omega^{mn}\Delta\Omega^{m'n'}\Delta V_{ij}\Phi^{mnm'n'}, \tag{13}$$

$$(C_{\text{em}}^{mn})_{ij} = k_{\text{a}}\Delta V_{ij}\Delta\Omega^{mn}, \tag{14}$$

$\Phi^{mnm'n'}$ is the averaged scattering phase function from the control solid angle $\Delta\Omega^{m'n'}$ to the control solid angle $\Delta\Omega^{mn}$.

The SPCU interpolation scheme [18] is used to express the intensities I_{p1l}^{mn} and I_{p2l}^{mn}, which appear in Eq. (7), in terms of nodal values of intensity.

For example, the value of the intensity on P_{1l} (Fig. 3b) is expressed as

$$I_{p1l}^{mn} = f_{1l}^{mn+} I_{p2l}^{mn} + (1 - f_{1l}^{mn+}) I_{N1l}^{mn} \quad \text{when } G_{1lN}^{mn} > 0, \tag{15}$$

$$I_{p1l}^{mn} = f_{1l}^{mn-} I_{p3l}^{mn} + (1 - f_{1l}^{mn-}) I_{N2l}^{mn} \quad \text{when } G_{1lN}^{mn} < 0, \tag{16}$$

where

$$f_{1l}^{mn+} = \text{Min}\left[\text{Max}\left(-\frac{G_{2lN}^{mn}}{G_{1lN}^{mn}}, 0\right), 1\right], \tag{17}$$

$$f_{1l}^{mn-} = \text{Min}\left[\text{Max}\left(-\frac{G_{3lN}^{mn}}{G_{1lN}^{mn}}, 0\right), 1\right]. \tag{18}$$

Using the following functions:

$$W_{klN}^{mn} = \text{Max}\left(\frac{G_{klN}^{mn}}{|G_{klN}^{mn}|}, 0\right), \quad k = 1, 2, 3 \tag{19}$$

the intensities $I_{p1l}^{mn}, I_{p2l}^{mn}$ and I_{p3l}^{mn} can be written in the following form:

$$I_{p1l}^{mn} = W_{1lN}^{mn}[f_{1l}^{mn+} I_{p2l}^{mn} + (1 - f_{1l}^{mn+}) I_{N1l}^{mn}] + (1 - W_{1lN}^{mn})[f_{1l}^{mn-} I_{p3l}^{mn} + (1 - f_{1l}^{mn-}) I_{N2l}^{mn}], \tag{20}$$

$$I_{p2l}^{mn} = W_{2lN}^{mn}[f_{2l}^{mn+} I_{p1l}^{mn} + (1 - f_{2l}^{mn+}) I_{N1l}^{mn}] + (1 - W_{2lN}^{mn})[f_{2l}^{mn-} I_{p3l}^{mn} + (1 - f_{2l}^{mn-}) I_{N3l}^{mn}], \tag{21}$$

$$I_{p3l}^{mn} = W_{3lN}^{mn}[f_{3l}^{mn+} I_{p2l}^{mn} + (1 - f_{3l}^{mn+}) I_{N3l}^{mn}] + (1 - W_{3lN}^{mn})[f_{3l}^{mn-} I_{p1l}^{mn} + (1 - f_{3l}^{mn-}) I_{N2l}^{mn}]. \tag{22}$$

Eqs. (20), (21) and (22) can assembled and written as follow:

$$I_{pl}^{mn} = [E_{lN}^{mn}] I_{Nl}^{mn}, \quad l = 1, 6, \tag{23}$$

where

$$[E_{lN}^{mn}] = [C_{lN}^{mn}]^{-1}[B_{lN}^{mn}], \tag{24}$$

$$[C_{lN}^{mn}] = \begin{bmatrix} 1 & -W_{1lN}^{mn} f_{1l}^{mn+} & -(1-W_{1lN}^{mn}) f_{1l}^{mn-} \\ -W_{2lN}^{mn} f_{2l}^{mn+} & 1 & -(1-W_{2lN}^{mn}) f_{2l}^{mn-} \\ -(1-W_{3lN}^{mn}) f_{3l}^{mn-} & -W_{3lN}^{mn} f_{3l}^{mn+} & 1 \end{bmatrix}, \tag{25}$$

$$[B_{lN}^{mn}] = \begin{bmatrix} W_{1lN}^{mn}(1-f_{1l}^{mn+}) & (1-W_{1lN}^{mn})(1-f_{1l}^{mn-}) & 0 \\ W_{2lN}^{mn}(1-f_{2l}^{mn+}) & 0 & (1-W_{2lN}^{mn})(1-f_{2l}^{mn-}) \\ 0 & (1-W_{3lN}^{mn})(1-f_{3l}^{mn-}) & W_{3lN}^{mn}(1-f_{3l}^{mn+}) \end{bmatrix}, \tag{26}$$

$$I_{pl}^{mn} = \begin{bmatrix} I_{p1l}^{mn} \\ I_{p2l}^{mn} \\ I_{p3l}^{mn} \end{bmatrix}, \tag{27}$$

$$I_{Nl}^{mn} = \begin{bmatrix} I_{N1l}^{mn} \\ I_{N2l}^{mn} \\ I_{N3l}^{mn} \end{bmatrix}. \tag{28}$$

Using the expressions of I_{p1l}^{mn} and I_{p2l}^{mn} given by Eq. (23), Eq. (7) becomes:

$$\sum_{l=1}^{6} \left[G_{1lN}^{mn} A_{1l}^{N} I_{p1l}^{mn} + G_{2lN}^{mn} A_{2l}^{N} I_{p2l}^{mn} \right] = \sum_{l=1}^{6} \sum_{k=1}^{3} \eta_{klN}^{mn} I_{Nkl}^{mn}, \tag{29}$$

where

$$\eta_{klN}^{mn} = G_{1lN}^{mn} A_{1l}^{N} (E_{lN}^{mn})_{1k} + G_{2lN}^{mn} A_{2l}^{N} (E_{lN}^{mn})_{2k}. \tag{30}$$

Replacing N by the superscript ij indicated in Fig. 3a, and using Eq. (29), the surfaces and angular integrals can be written as

$$\begin{aligned} &\sum_{l=1}^{6} \left[\int_{\Delta\Omega^{mn}} \int_{M_l}^{G_l} \boldsymbol{J} \cdot \boldsymbol{n} \, \mathrm{d}s \, \mathrm{d}\Omega + \int_{\Delta\Omega^{mn}} \int_{G_l}^{M_{l+1}} \boldsymbol{J} \cdot \boldsymbol{n} \, \mathrm{d}s \, \mathrm{d}\Omega \right]_{ij} \\ &\quad = \gamma_{1ij}^{mn} I_{i-1j-1}^{mn} + \gamma_{2ij}^{mn} I_{i-1j}^{mn} + \gamma_{3ij}^{mn} I_{ij-1}^{mn} + \gamma_{7ij}^{mn} I_{ij}^{mn} + \gamma_{4ij}^{mn} I_{ij+1}^{mn} + \gamma_{5ij}^{mn} I_{i+1j}^{mn} + \gamma_{6ij}^{mn} I_{i+1j+1}^{mn}, \end{aligned} \tag{31}$$

where

$$\gamma_{1ij}^{mn} = \eta_{15ij}^{mn} + \eta_{26ij}^{mn}, \tag{32}$$

$$\gamma_{2ij}^{mn} = \eta_{34ij}^{mn} + \eta_{25ij}^{mn}, \tag{33}$$

$$\gamma_{3ij}^{mn} = \eta_{21ij}^{mn} + \eta_{36ij}^{mn}, \tag{34}$$

$$\gamma_{4j}^{mn} = \eta_{33ij}^{mn} + \eta_{24ij}^{mn}, \tag{35}$$

$$\gamma_{5ij}^{mn} = \eta_{31ij}^{mn} + \eta_{22ij}^{mn}, \tag{36}$$

$$\gamma_{6ij}^{mn} = \eta_{32ij}^{mn} + \eta_{23ij}^{mn}, \tag{37}$$

$$\gamma_{7ij}^{mn} = \sum_{l=1}^{6} \eta_{1lij}^{mn}. \tag{38}$$

Replacing expressions of several terms of Eq. (5) by their developed expressions given by Eqs. (8), (9), (10) and (31), the resulting algebraic equations have the following form:

$$\gamma_{1ij}^{mn} I_{i-1j-1}^{mn} + \gamma_{2ij}^{mn} I_{i-1j}^{mn} + \gamma_{3ij}^{mn} I_{ij-1}^{mn} + \alpha_{ij}^{mnmn} I_{ij}^{mn} + \gamma_{4ij}^{mn} I_{ij+1}^{mn} + \gamma_{5ij}^{mn} I_{i+1j}^{mn} + \gamma_{6ij}^{mn} I_{i+1j+1}^{mn} = S_{ij}^{mn}, \tag{39}$$

where

$$S_{ij}^{mn} = \beta_{ij}^{mn} - \sum_{(m',n')\neq(m,n)} (\alpha_{ij}^{mnm'n'} I_{ij}^{m'n'}), \tag{40}$$

$$\alpha_{ij}^{mnm'n'} = \begin{cases} \left(\gamma_{7ij}^{mn} - \left(C_{\text{ex}}^{mn}\right)_{ij} - \left(C_{\text{diff}}^{mnmn}\right)_{ij}\right) & \text{if } (m',n') = (m,n), \\ -\left(C_{\text{diff}}^{mnm'n'}\right)_{ij} & \text{if } (m',n') \neq (m,n), \end{cases} \tag{41}$$

$$\beta_{ij}^{mn} = \left(C_{\text{em}}^{mn}\right)_{ij} I_{bij}^{mn}. \tag{42}$$

The integration of the RTE (Eq. (1)) over a boundary control volume V_{ij} (Fig. 3a) and a control solid angle Ω^{mn} is calculated using the same strategy adopted for an interior control volume and with taking into account the boundaries wall contribution given by Eq. (2). The obtained discretized equation for the boundaries nodes are expressed easily on the same form as Eq. (39). The source term and the coefficients $\alpha_{ij}^{mnm'n'}$ depend on wall properties.

It is clear that in the discretized RTE obtained by CVFEM (Eq. (39)), six nodes are used for each calculation point instead of four nodes when FVM is used, therefore, the accuracy of the numerical resolution process is improved.

3.2. Resolution method

Due to the non-linearity (dependence of the source term on the intensities) of the discretized RTE obtained by the different numerical methods of discretization (DOM, FVM, CVFEM), several iterative techniques in which coefficients are computed using the latest available values of the intensities, are employed to solve the algebraic systems.

Using the FV Method, Chai et al. [14] have studied some radiative heat transfer problems. In their work, the authors have used the step and exponential interpolation schemes and they

obtained, in the case of two-dimensional problem, the following discretized RTE :

$$I_p^\ell = \alpha_W^\ell I_W^\ell + \alpha_S^\ell I_S^\ell + S_P^\ell, \tag{43}$$

where S_P^ℓ represents the source term which depends on the intensities.

Eq. (43) is established for $Dc_x^\ell > 0$ and $Dc_y^\ell > 0$. The same form is obtained for the other directions.

In the solution of Eq. (43), with appropriate boundaries conditions, zero intensity or a suitable intensity filed is used as an initial guess. The solution process is initiated with the $Dc_x^\ell > 0$ and $Dc_y^\ell > 0$ conditions by a marching process. This process is repeated for all other directions, and a solution is deemed converged when it satisfied a specific constraint.

Baek and Kim [16], and Moder et al. [15] have employed the FV Method and step interpolation scheme to analysis the radiative heat transfer in cylindrical problems. The obtained discretized RTE in their works has the following form:

$$I_p^\ell = \alpha_W^\ell I_W^\ell + \alpha_S^\ell I_S^\ell + \alpha_E^\ell I_E^\ell + \alpha_N^\ell I_N^\ell + \alpha_B^\ell I_B^\ell + \alpha_T^\ell I_T^\ell + S_P^\ell, \tag{44}$$

where the source term depends on the intensities in the other directions $\ell'(\ell' \neq \ell)$.

This discretized equation has been solved using the same technique employed by Chai et al. [14].

It is important to note that the use of this technique which begins from boundaries conditions, is justified only when the outgoing intensities at the boundaries are independent of the incoming radiations (the boundaries surfaces of the physical domain are black). Hence, when the boundaries surfaces are not black problem of oscillation and/or divergence can be confronted.

In their study concerning the development of an unstructured radiation model, Liu et al. [17], have used the FVM and step scheme to discretize the RTE. They obtained M systems of non symmetric algebraic equations (M represents number of directions). Each system represents the spatial discretization in one discrete direction and is solved independently. Due to the dependence of the source term and boundaries conditions on the intensities, global iteration is used. As the first step of solution procedure, an initial solution is assumed and used to calculate the source term. Then a system of spatially discretized equations is solved for each direction.

Rousse [13] has applied CVFEM as a new technique to discretize the RTE. He obtained a discretized equation that has the same form as the equation obtained in the present work (Eq. (39)). The TDMA technique is used by the author to solve the algebraic system.

For all the previous studies, authors reclaim problems of convergence, oscillation and CPU time when there are reflecting boundaries surfaces and/or in-scattering. These problems can be attributed to the interpolation schemes, the resolution techniques, and essentially to the formulation of the discretized RTE and in particularly when the in-scattering contribution term is considered in the source term.

To avoid these problems we propose a new formulation of the CVFEM discretized RTE in which the source term depends only on temperature. The algebraic system is expressed as follow:

$$\gamma_{1ij}^{mn} I_{i-1j-1}^{mn} + \gamma_{2ij}^{mn} I_{i-1j}^{mn} + \gamma_{3ij}^{mn} I_{ij-1}^{mn} + \sum_{(m',n')=(1,1)}^{(N_\theta,N_\varphi)} (\alpha_{ij}^{mnm'n'} I_{ij}^{m'n'}) + \gamma_{4ij}^{mn} I_{ij+1}^{mn} + \gamma_{5ij}^{mn} I_{i+1j}^{mn} + \gamma_{6ij}^{mn} I_{i+1j+1}^{mn} = S_{ij}^{mn}, \tag{45}$$

where the source term, S_{ij}^{mn}, is defined as $S_{ij}^{mn} = \beta_{ij}^{mn}$

It is very important to note that the terms $\gamma_{kij}^{mn}, \alpha_{ij}^{mnm'n'}$ and β_{ij}^{mn} depend only on physical properties, geometrical coefficients and temperature. Also, we note that Eq. (45) contains seven spatial unknown intensities in direction (m,n) and $(N_\theta N_\varphi - 1)$ unknown intensities in the other directions (m',n'). Consequently, the direction dependence between intensities is respected.

The proposed formulation permits us to solve the algebraic system by a direct method or an iterative method in which all the intensities (I_{ij}^{mn}) are calculated simultaneously after each iteration and the convergence is guaranteed. These methods requires the establishment of a matrix system.

3.3. Matrix formulation

In order to formulate the matrix system of the discretized equations, the radiation intensity I_{ij}^{mn} on point N defined by (i,j) and in direction of propagation (m,n) will be represented by $I(l)$ where l is expressed in terms of i,j,m and n as follow:

$$l = (i-1)N_y N_\theta N_\varphi + (j-1)N_\theta N_\varphi + (m-1)N_\theta + n. \tag{46}$$

Using this definition of the intensity vector I, the algebraic equations (47) can be written in the following matrix form:

$$AI = b, \tag{47}$$

where A is a square matrix having $(N_x \times N_y \times N_\theta \times N_\varphi)^2$ coefficients which are given by

$$A_{lk} = \begin{cases} \alpha_{ij}^{mnm'n'} & \text{if } k = k_\alpha, \\ \gamma_{1ij}^{mn} & \text{if } k = k_{\gamma 1}, \\ \gamma_{2ij}^{mn} & \text{if } k = k_{\gamma 2}, \\ \gamma_{3ij}^{mn} & \text{if } k = k_{\gamma 3}, \\ \gamma_{4ij}^{mn} & \text{if } k = k_{\gamma 4}, \\ \gamma_{5ij}^{mn} & \text{if } k = k_{\gamma 5}, \\ \gamma_{6ij}^{mn} & \text{if } k = k_{\gamma 6}, \\ 0 & \text{if not,} \end{cases} \tag{48}$$

where

$$\begin{aligned} k_\alpha &= (i-1)N_y N_\theta N_\varphi + (j-1)N_\theta N_\varphi + (m'-1)N_\theta + n', \\ k_{\gamma 1} &= (i-2)N_y N_\theta N_\varphi + (j-2)N_\theta N_\varphi + (m-1)N_\theta + n, \\ k_{\gamma 2} &= (i-2)N_y N_\theta N_\varphi + (j-1)N_\theta N_\varphi + (m-1)N_\theta + n, \\ k_{\gamma 3} &= (i-1)N_y N_\theta N_\varphi + (j-2)N_\theta N_\varphi + (m-1)N_\theta + n, \\ k_{\gamma 4} &= (i-1)N_y N_\theta N_\varphi + jN_\theta N_\varphi + (m-1)N_\theta + n, \\ k_{\gamma 5} &= iN_y N_\theta N_\varphi + (j-1)N_\theta N_\varphi + (m-1)N_\theta + n, \\ k_{\gamma 6} &= iN_y N_\theta N_\varphi + jN_\theta N_\varphi + (m-1)N_\theta + n \end{aligned} \tag{49}$$

and $l = 1 \ldots N_x N_y N_\theta N_\varphi$

The term b which appears in Eq. (47) represents the vector that contains the medium and the boundaries emission contributions. The coefficients of this vector are given by

$$b(l) = \beta_{ij}^{mn}. \tag{50}$$

The relation between l and (i,j,m,n) is given by Eq. (46).

This matrix formulation of the discretized RTE permits the use of many iterative method employed in CFD such as Conjugate Gradient methods, Lanczos method, Jaccobi method.

In the present work, the obtained matrix system is solved using the conditioned conjugate gradient squared method (CCGS).

On the other hand, the necessary volume of the memory to stock matrix coefficients represents one of the problem especially when the matrix dimension is very large. (For example: in this work the matrix dimensions are equal to $172,800 \times 172,800$.) So a computational technique is necessary to avoid the storage of zero-coefficients. For this reason, the YSMP storage technique is used.

4. Results and discussion

4.1. Validation

In order to assess the validity of the proposed methodology and the associated computer program, several test problems are considered. In these test problems, the wall bounding the physical domain is assumed grey and emits and reflects diffusely radiation.

4.1.1. Grey scattering media

In the enclosure depicted in Fig. 1 surface 1 is maintained at a constant temperature, T_1, and all other surfaces are assumed to be at a constant zero temperature, $T_2 = T_3 = T_4 = 0$. The medium is assumed to scatter radiation isotropically and does not absorb radiant energy ($k_a = 0$).

The effects of wall emissivities and optical thickness on the dimensionless radiant heat flux, $Q_r(Q_r = q_r/\sigma T_1^4)$, at the lower surface (wall 1) are presented in Figs. 4 and 5. The radiant heat flux distribution is symmetric with respect to a vertical centreline, thus results are presented only for $0 \leqslant x \leqslant 0.5$. It is seen that our results agree satisfactorily with those mentioned in literature [19].

As the emissivity decreases, the intensity leaving a boundary becomes increasingly dependent on the incident intensity on this boundary: as a result, the radiant heat flux at the hot wall becomes increasingly uniform and small with decreasing ε.

4.1.2. Grey absorbing and non-scattering media

In this test case the proposed algorithm is applied to rectangular enclosure filled with an absorbing medium at constant temperature T_m. The walls temperature is set equal to zero ($T_1 = T_2 = T_3 = T_4 = 0$).

Fig. 6 illustrates the effect of the medium optical thickness, τ, on the dimensionless radiant heat flux and shows that the present solutions are in good agreement with the proposed reference solutions. As τ increases, the intensity at any particular point becomes increasingly dependent of

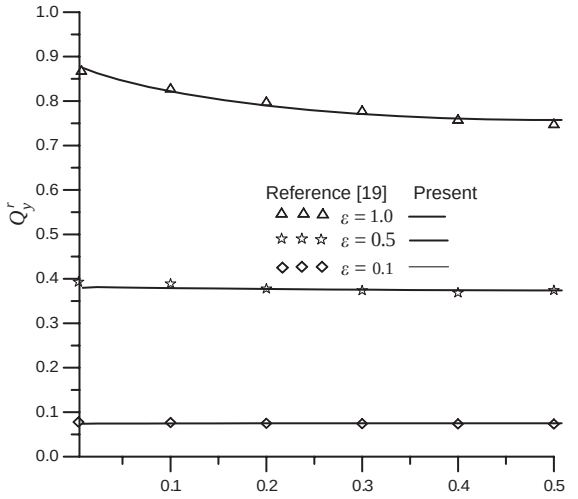

Fig. 4. Effects of wall emissivities on the dimensionless radiant heat flux in the case of *Grey scattering media* ($L_x/L_y = 1, \tau = 1$).

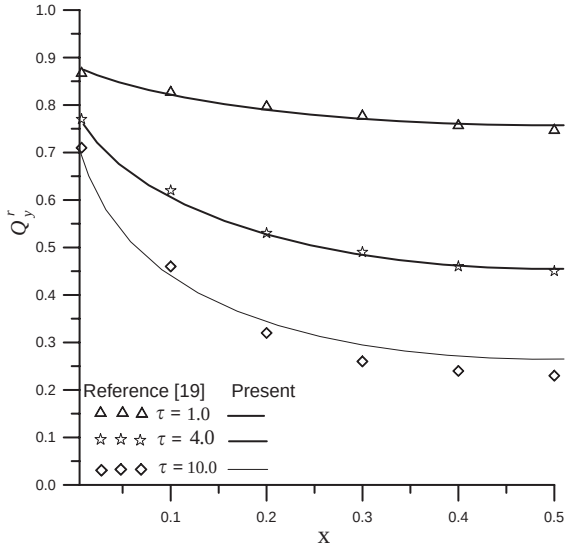

Fig. 5. Effects of optical thickness on the dimensionless radiant heat flux in the case of *Grey scattering media* ($L_x/L_y = 1, \varepsilon = 1$).

its immediate surrounding. For a boundary point, N, the incoming intensity is then related to the intensity of a point in the medium very near N. As the boundary temperature is zero (zero out going radiant heat flux) and the medium temperature is T_m, for $\tau = 10$, Q_r, is approximately unity.

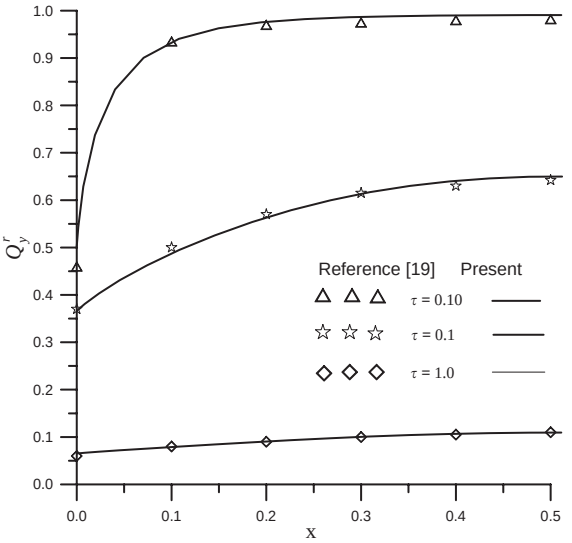

Fig. 6. Effects of optical thickness on the dimensionless radiat heat flux in the case of *Grey absorbing media* ($L_x/L_y = 1, \varepsilon = 1$).

4.2. *Effects of radiative parameters on spatial distribution of radiant heat flux*

In order to understand more the radiative heat transfer in participant medium, the spatial distribution of the radiant heat flux is presented for different cases.

Fig. 7 indicates that, when the enclosure is filled by an absorbing medium maintained at a constant temperature, T_m, and with cold walls ($T_w < T_m$), radiant heat flux in y-direction depends strongly on the optical thickness. On the one hand, it is noted that near the walls the flux becomes evidently much higher as τ increases. This result can be explained by the fact that when absorbing coefficient is large the medium emits more radiative energy. On the other hand, it is interesting to note that there is a critical value τ_c of the optical thickness τ. When $\tau < \tau_c$ (Fig. 7), the radiant heat flux in all over the media except near the wall increases with τ and it decreases with the increasing of τ in the other range values ($\tau > \tau_c$). The existence of this critical value can be explained by the presence of the two antagonistic media emission and absorption radiative phenomena.

It is noticed that when the wall emissivity decreases, the y-direction radiant flux in all the media decreases (Fig. 8).

For all the considered values of the optical thickness and wall emissivities, the radiant heat flux at $y = 0.5$ is equal to zero because of the problem symmetry.

The spatial evolution of the radiant heat flux within a purely scattering medium and for different values of optical thickness and walls emissivities are presented, respectively, in Figs. 9 and 10. Surface 1 (Fig. 1) is maintained at a constant temperature, T_1, and all other surfaces are assumed to be at a constant zero temperature, $T_2 = T_3 = T_4 = 0$. The obtained profiles show that the radiant heat flux leaving the hot wall and within the media decreases with τ. This effect is related to the amount of radiative energy scattered by the medium to the heated wall. In addition,

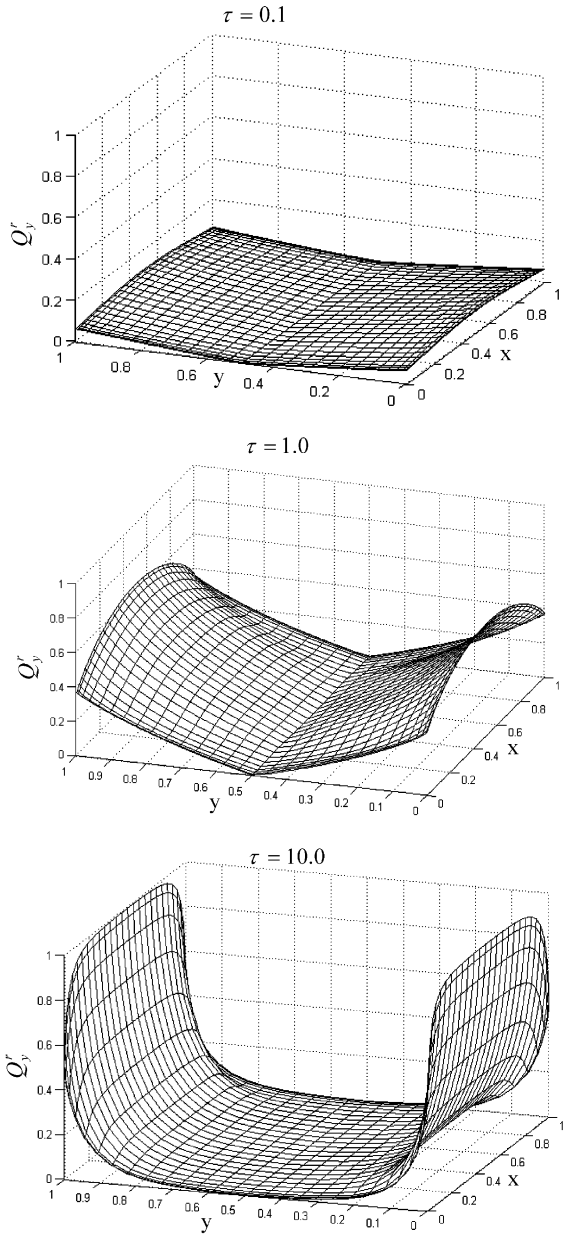

Fig. 7. Spatial evolution of y-direction radiant heat flux within the cavity for different values of optical thickness (*Grey absorbing media and black wall*).

we note that the amplitude of this flux in all the media is increasingly dependent on the emissivities of the enclosure's contours (Fig. 10).

The radiative energy propagation within a participating medium can be easily analysed from the vectorial distribution of total radiant heat flux. For this reason we presented the flux vector for different physical problems (Fig. 11).

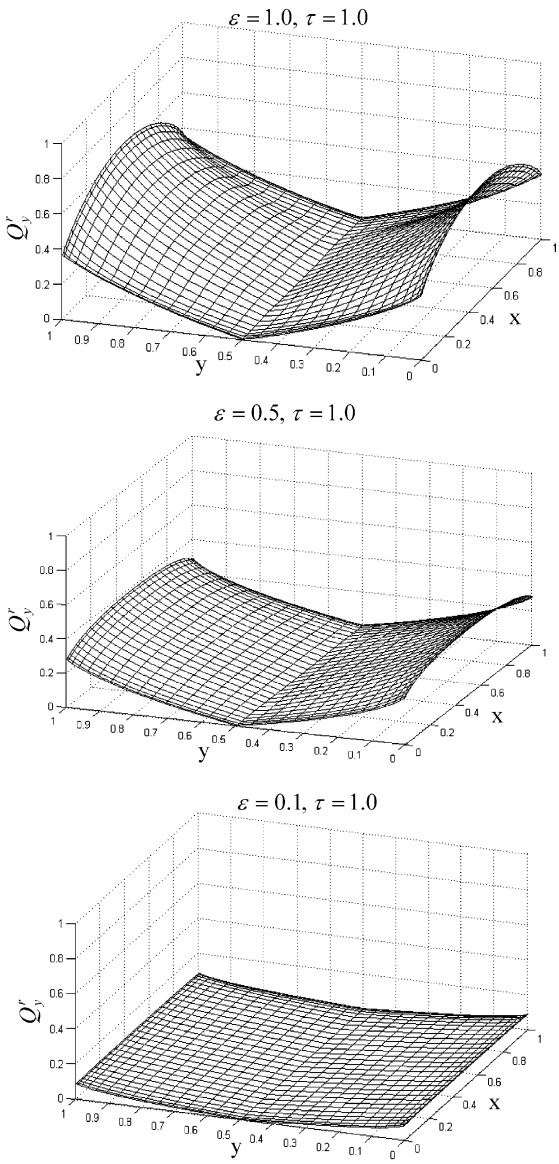

Fig. 8. Spatial evolution of y-direction radiant heat flux within the cavity for different values of wall emissivities (*Grey absorbing media*).

4.3. Comparison between TDMA and CCGS resolution methods

Table 1 lists the required CPU time and number of iterations needed by the TDMA and CCGS solvers to obtain a convergent solution for the case of an absorbing and emitting media problem and purely scattering media problem.

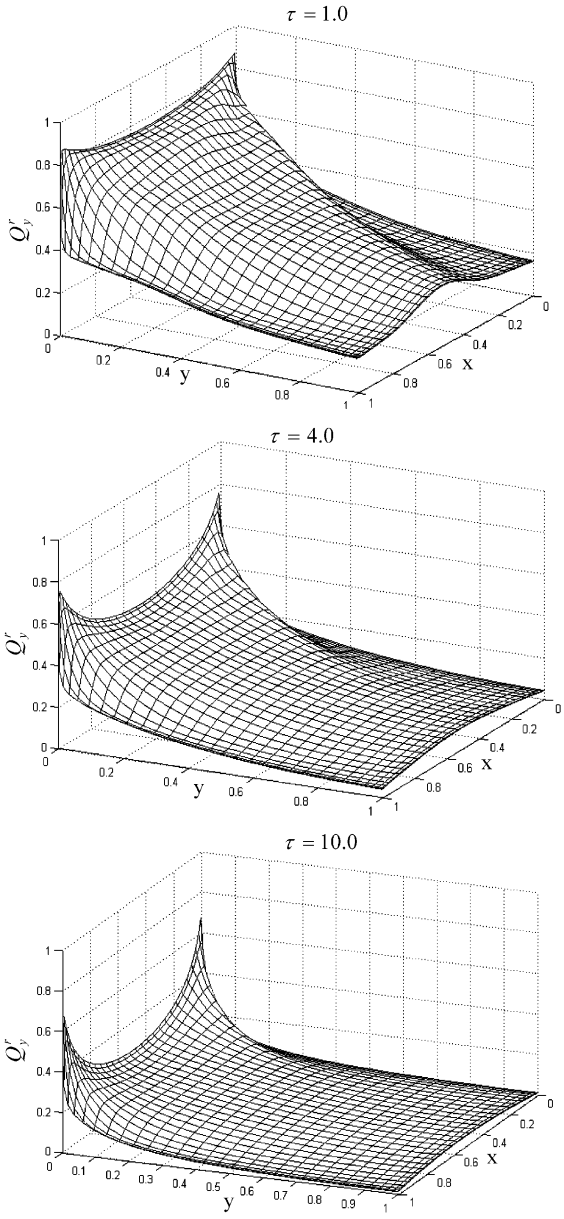

Fig. 9. Spatial evolution of *y*-direction radiant heat flux within the cavity for different values of optical thickness (*Grey scattering media and black wall*).

It is noted that, for the first problem, the number of iterations for these two solvers are essentially the same, however, the CCGS method requires about 2.4% of the TDMA needed CPU time.

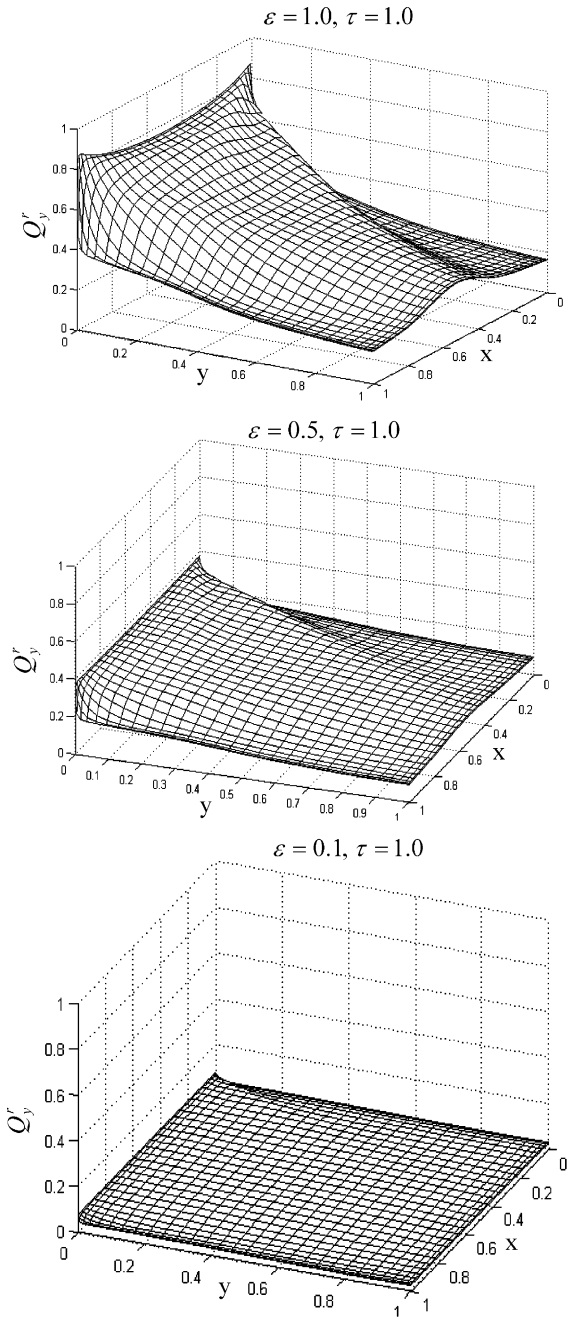

Fig. 10. Spatial evolution of y-direction radiant heat flux within the cavity for different values of wall emissivities (*Grey scattering media*).

When the in-scattering contribution is considered in the source term a non-linear algebraic system is obtained. This non-linearity leads to a large changes in the predicted solutions between successive iterations especially for high optical thickness. Also, this changes is even important when TDM algorithm, in which source term is computed using the latest available values of intensities, is used. For this reason, the number of iterations needed by TDMA solver increases with τ as indicated in Table 1.

However, it is noticed that, in spite of the important effect of the in-scattering when τ is large, there is no significant variation of iterations and CPU time when the CCGS solver and the new formulation, proposed in this paper, are used. In particularly, it can be seen that, for the purely scattering problem, the processing time ratio of the TDM and CCGS algorithms changes from 3 to 38 for $\tau = 1-10$, respectively.

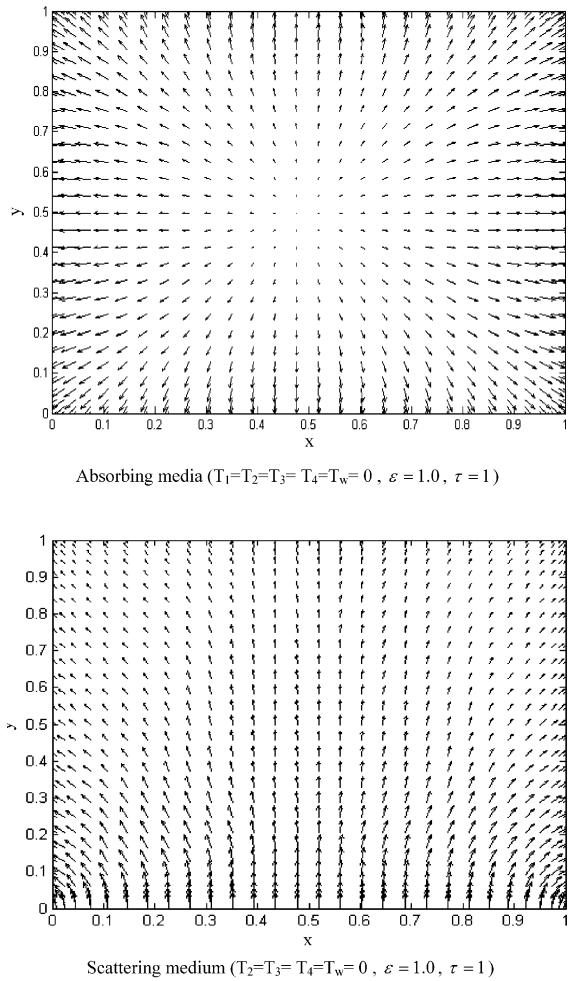

Fig. 11. Vectorial distribution of total radiant heat flux within the rectangular cavity.

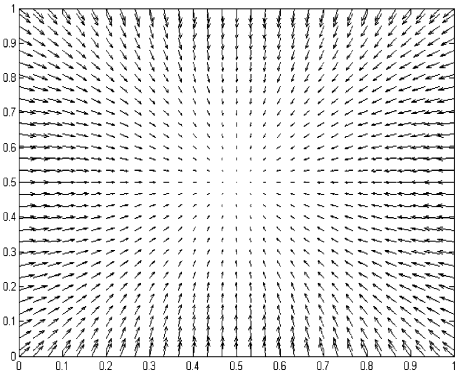

Absorbing and Scattering medium ($T_1=T_2=T_3=T_4=T_w$, $T_m<T_w$, $\varepsilon = 0.8$, $\tau = 1$)

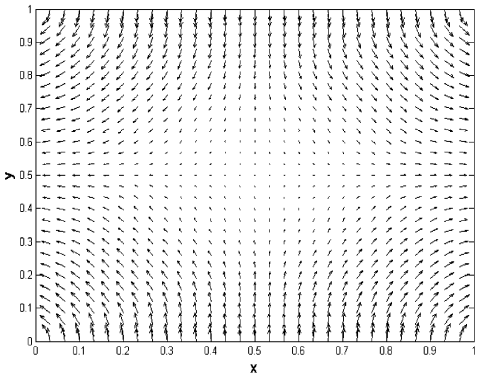

Absorbing and Scattering medium ($T_1=T_3$, $T_m<T_1$, $T_4=T_2=0$, $\varepsilon = 0.8$, $\tau = 1$)

Fig. 11. (*Continued*)

Table 1
CPU time and iterations

	Optical thickness τ	TDMA		CCGS	
		CPU time (s)	Iterations	CPU time (s)	Iterations
Grey absorbing and non-scattering media with black wall	1	15.0	27	0.41	32
	5	16.2	30	0.40	29
	10	16.3	30	0.39	27
Grey scattering media with black wall	1	14.0	27	5.50	68
	5	70.0	130	5.40	66
	10	189.0	358	5.20	64

5. Conclusion

A new methodology for the numerical treatment of radiative heat transfer in emitting, absorbing and scattering media is presented. This methodology is based on the discretization of the Radiative Transfer Equation by CVFEM, and conditioned conjugate gradient squared method (CCGS) for solving the obtained discretized equations.

The validity of the present solutions has been tested by comparison with available works [19]. A good agreement is obtained. In addition, the proposed formulation makes it possible to solve the discretized RTE by direct method, and proves to be very accurate and of good flexibility and its implementation in the other numerical procedures used for the resolution of fluid dynamics and convection–conduction problems is conceptually easy.

The numerical simulation of radiative heat transfer for different cases using the proposed algorithm has shown that the developed computer program needs an accurate CPU time and is exempt of any numerical oscillations.

References

[1] Hottel HC, Cohen ES. Radiant heat exchanges in gas-filled enclosure: allowance for non-uniformity of gas temperature. AIChE J 1958;4:3–14.
[2] Hottel HC, Sarofim AF. Radiative transfer. New-York: McGraw-Hill; 1967.
[3] Howell JR. Application of Monte-Carlo methods to heat transfer problems. Adv Heat Transfer 1969;5.
[4] Haji-Sheikh A. Monte-Carlo methods. In: Minkowycz WJ, Sparrow EM, Schneider GE, Pletcher RH editors. Handbook of numerical heat transfer. NewYork: Wiley; 1988. p. 421–61 [chapter 16].
[5] Halton JH. A retrospective and prospective review of the Monte-Carlo method. SIAM Rev 1990;12(1):1–63.
[6] Shah N. The computation of radiation heat transfer. PhD thesis. Imperial College, London, 1979.
[7] Meng FL, Mckenty F, Camarero R. Radiative heat transfer by the discrete transfer method using an unstructured mesh. In: HTD-Vol.244, Radiative heat transfer: theory and applications. New York: ASME; 1993. p. 55–66.
[8] Carvalho MG, Farias T, Fontes P. Predicting radiative heat transfer in absorbing, emitting, and scattering media using the discrete transfer method. In: HTD Vol. 160, Fundamentals of radiation heat transfer. New York: ASME; 1991. p. 17–26.
[9] Chandrasekhar S. Radiative transfer. Oxford: Clarendon Press; 1950.
[10] Carlson BG, Lathrop KD. Transport theory—the method of discrete-ordinates. In: Computing methods in reactor physics. New York: Gordon & Breach; 1968.
[11] Chai JC, Patankar SV, Lee HS. Evaluation of spatial differencing practices for the discrete-ordinates method. J Thermophys Heat Transfer 1994;8(1):140–4.
[12] Rousse DR, Baliga RB. Formulation of a control-volume finite element method for radiative transfer in participating media. In: Proceedings of the seventh international conference on numerical methods thermal problems. Stanford; 1991. p. 786–95.
[13] Rousse DR. Numerical prediction of two-dimensional conduction, convection, and radiation heat transfer. I—formulation. Int J Therm Sci 2000;39:315–31.
[14] Chai JC, Lee HS, Patankar SV. Finite volume method for radiation heat transfer. J Thermophys Heat Transfer 1994;8(3).
[15] Moder JP, Chai JC, Parthasarathy G, Lee HS, Patankar SV. Nonaxisymmetric radiative transfer in cylindrical enclosures. Numer Heat Transfer, Part B 1996;30:437–52.
[16] Baek SW, Kim MY. Analysis of radiative heating of a rocket plume base with the finite-volume method. Int J Heat Mass Transfer 1997;40(7):1501–8.

[17] Liu J, Shang HM, Chen YS. Development of an unstructured radiation model applicable for two-dimensional planar, axisymmetric, and three-dimensional geometries. J Quant Spectrosc Radiat Transfer 2000;66:17–33.
[18] Rousse DR, Gautier G, Sacadura JF. Une fonction d'interpolation produisant des coefficients positifs pour le rayonnement. Cong Français Thermique SFT 2000, 15–17 mai 2000.
[19] Rousse DR, Gautier G, Sacadura JF. Numerical prediction of two-dimensional conduction, convection, and radiation heat transfer. II—validation. Int J Therm Sci 2000;39:332–53.